GPR56/ADGRG1 is a platelet collagen-responsive GPCR and hemostatic sensor of shear force

Jennifer Yeung[a], Reheman Adili[a], Emily N. Stringham[a], Rong Luo[b], Alexander Vizurraga[a], Luciana K. Rosselli-Murai[a], Hannah M. Stoveken[a], Maiya Yu[a], Xianhua Piao[b,c], Michael Holinstat[a,d], and Gregory G. Tall[a,1]

[a]Department of Pharmacology, University of Michigan Medical Center, Ann Arbor, MI 48109; [b]Department of Medicine, Boston Children's Hospital and Harvard Medical School, Boston, MA 02115; [c]Newborn Brain Research Institute, Department of Pediatrics, Weill Institute for Neuroscience, University of California, San Francisco, CA 94158; and [d]Department of Internal Medicine, Division of Cardiovascular Medicine, University of Michigan Medical Center, Ann Arbor, MI 48109

Edited by Robert J. Lefkowitz, Howard Hughes Medical Institute, Durham, NC, and approved September 14, 2020 (received for review May 6, 2020)

Circulating platelets roll along exposed collagen at vessel injury sites and respond with filipodia protrusion, shape change, and surface area expansion to facilitate platelet adhesion and plug formation. Various glycoproteins were considered to be both collagen responders and mediators of platelet adhesion, yet the signaling kinetics emanating from these receptors do not fully account for the rapid platelet cytoskeletal changes that occur in blood flow. We found the free N-terminal fragment of the adhesion G protein-coupled receptor (GPCR) GPR56 in human plasma and report that GPR56 is the platelet receptor that transduces signals from collagen and blood flow-induced shear force to activate G protein 13 signaling for platelet shape change. *Gpr56*$^{-/-}$ mice have prolonged bleeding, defective platelet plug formation, and delayed thrombotic occlusion. Human and mouse blood perfusion studies demonstrated GPR56 and shear-force dependence of platelet adhesion to immobilized collagen. Our work places GPR56 as an initial collagen responder and shear-force transducer that is essential for platelet shape change during hemostasis.

hemostasis | platelets | adhesion GPCR | collagen | signal transduction

Hemostasis is the physiological wound healing process that prevents blood loss while maintaining normal blood flow. Platelets are anucleate cell fragments that serve as major contributors to hemostatic plug formation. The process is initiated by platelet surface receptor engagement with subendothelial collagen of the extracellular matrix that becomes exposed during vessel wall injury (1–3). The initiating hemostatic step involves platelet glycoprotein Ibα (GPIbα) transiently tethering to collagen-bound von Willebrand factor (vWF) (2–5). A multistep mechanism ensues in which multiple receptors including glycoprotein VI (GPVI) and integrin $\alpha_2\beta_1$ participate in platelet spreading, activation, stable adhesion, and the aggregation events that are necessary to support thrombus growth (6–8). Within the sequential activating events, tethered platelets undergo rapid reorganization of the cytoskeletal structure, expanding from discoid to spherical shapes in order to spread over the damaged surface (9). Actin polymerization within platelets permits the development and extension of filopodia protrusions and lamellipodia that enable platelet deceleration in the blood flow, flattening and stable adhesion. Activated platelets release storage granule contents, including autocrine and paracrine platelet agonists that fulfill the platelet activation process (2, 10, 11). These events are prerequisite to secondary platelet recruitment and formation of stable clots.

Dynamic glycoprotein receptor interactions with collagen have been viewed as the dominant initiating events leading to platelet plug formation. Arteriole injury and platelet activation experiments using a GPVI-deficient mouse model showed defects in hemostatic plug formation and platelet adhesion to collagen (12, 13). However, additional measures demonstrated that GPVI-deficient mice have negligibly prolonged bleeding times and no impairment in induced occlusive thrombus formation (14–16). The differences in the experimental approaches used to investigate platelet responses to collagen have offered varied interpretations of whether GPVI is the key signaling receptor that acts to initiate platelet activation (2, 7, 8, 13). For example, exogenous collagen promotes sustained GPVI/Fc Receptor gamma (FcRγ) signaling through phospholipase Cγ2 (PLCγ2), but the Ca^{+2} mobilization output and kinetics of this multistep signaling pathway may not fully account for the quick-onset cytoskeletal changes that are required for platelet deceleration in rapid blood flow (1, 17). Thus, the putative existence of other rapid-acting platelet collagen receptors has been considered. These receptor(s) may be engaged prior to or concomitantly with the glycoprotein collagen receptors (7).

Heterotrimeric G protein 13 (G13) signaling is required to stimulate the cytoskeletal-dependent platelet shape changes in response to collagen (18). Gα13-GTP (guanosine triphosphate) rapidly and robustly activates Rho family small G protein signaling to induce actin polymerization (19). Accounting for the means of G13 activation is not readily explained by the actions of the current repertoire of platelet collagen receptors. Here, we identified the collagen-responsive, G13-coupled, G protein-coupled receptor (GPCR) GPR56 or ADGRG1 on the surface of platelets (20–23). GPR56 is an adhesion G protein-coupled receptor

Significance

We identified the known collagen receptor GPR56/ADGRG1 on platelets. GPR56 is an adhesion G protein-coupled receptor that becomes activated following forced dissociation of its N-terminal fragment and C-terminal fragment or seven-transmembrane spanning domain (7TM). Fragment dissociation reveals the cryptic stalk of the 7TM, which acts as a tethered peptide agonist, and for GPR56, this activates platelet G13 signaling. GPR56 pharmacological probes activated platelets to undergo shape change and aggregation, which are critical for the formation of hemostatic plugs. *Gpr56*$^{-/-}$ mice exhibit prolonged bleeding, defective platelet plug formation in vessel injury assays, and delayed thrombotic vessel occlusion. Shear-force dependency of platelet adhesion to immobilized collagen was found to be GPR56 dependent.

Author contributions: J.Y., A.V., L.K.R.-M., H.M.S., and G.G.T. designed research; J.Y., R.A., E.N.S., A.V., L.K.R.-M., H.M.S., M.Y., and G.G.T. performed research; J.Y., R.L., X.P., and G.G.T. contributed new reagents/analytic tools; J.Y., E.N.S., A.V., L.K.R.-M., H.M.S., M.H., and G.G.T. analyzed data; and J.Y. and G.G.T. wrote the paper.

The authors declare no competing interest.

This article is a PNAS Direct Submission.

[1]To whom correspondence may be addressed. Email: gregtall@med.umich.edu.

This article contains supporting information online at https://www.pnas.org/lookup/suppl/doi:10.1073/pnas.2008921117/-/DCSupplemental.

First published October 23, 2020.

(AGPCR), a receptor subclass distinguished by the presence of a GPCR autoproteolysis-inducing domain that self-cleaves the receptors at a precise extracellular site proximal to the start of the first transmembrane span (TM1) of the seven-transmembrane bundle (24). Self-cleavage is constitutive, and the two resulting receptor pieces, termed the N-terminal fragment (NTF) and C-terminal fragment (CTF), remain noncovalently bound. Recent biochemical evidence demonstrated that dissociation of the two receptor fragments resulted in strong activation of G protein signaling (22, 23). Dissociation of the NTF unveils a stalk peptide emanating from TM1 that acts as a tethered peptide agonist to activate the CTF (23, 25). One proposed physiological mechanism of AGPCR activation is through shear force-mediated NTF/CTF dissociation. The NTF becomes immobilized to its protein ligand, and the force created by cell movement drives the dissociation event. Our work shows that GPR56 is a platelet collagen GPCR that has the critical role of providing early-onset G13 activation to facilitate the platelet shape changes and integrin activation that are necessary for efficient hemostasis and thrombosis.

Results

The Identification of Collagen-Binding Adhesion GPCR NTFs in Human Plasma. Most of the 33 AGPCRs are orphans, but 2 that were deorphanized have collagen subtypes as physiological ligands, GPR56/ADGRG1 and GPR126/ADGRG6 (21, 26). Upon blood vessel wall injury, the subendothelial layer of collagen becomes exposed to the blood flow and exerts profound influence on circulating cells, particularly platelets (2). One hypothesized AGPCR activation mechanism is that the NTFs become anchored to their extracellular matrix ligand(s), and shear force created by cell movement serves to dissociate the NTF and CTF to instigate tethered agonism and consequent G protein signaling (23, 27, 28) (Fig. 1*A*). We postulated that if cells in circulation (i.e., shear flow) express collagen-regulated AGPCRs, they might shed their NTF(s) onto exposed collagen, after which it could be liberated to the plasma for clearance. Collagen-coated bead protein pull-down experiments were performed using clarified human plasma, followed by shotgun mass spectrometry and sodium dodecyl sulfate (SDS)/polyacrylamide gel electrophoresis (PAGE) analyses. Many known collagen-binding proteins were identified with high confidence, including fibrinogens, vWF, various integrins, and the AGPCR, ADGRG1/GPR56 (Datasets S1 and S2 and *SI Appendix*, Table S1) (21, 29). One tryptic peptide of the collagen IV-binding AGPCR NTF of GPR126/ADGRG6 was also found (26). Intriguingly, no tryptic peptides corresponding to the GPR56 CTF were found in the pull downs of plasma, yet 11 tryptic peptides from the GPR56 NTF were identified (Fig. 1*B*, Dataset S3, and *SI Appendix*, Fig. S1), indicating that the GPR56 NTF present in plasma was likely shed from a circulating cell or conceivably from a cell type that comprises vessel walls. GPR56 immunoblot analysis verified that the endogenous GPR56 NTF from plasma and purified recombinant GPR56 NTF (hereto referred as GPR56 rNTF), a 40-kDa glycosylated protein containing a collagen-binding Pentraxin/Laminin/neurexin/sex hormone-binding globulin-like (PLL) domain, was bound to the collagen beads (21, 30). No GPR56 CTF was observed in the collagen pull downs of plasma (Fig. 1*C*).

GPR56 Is a Platelet-Resident GPCR That Activates G13 and G protein i (Gi) but Not G protein q (Gq) Signaling. As circulating platelets are highly responsive to collagen during hemostasis, we probed platelets for the GPR56 NTF identified in the human plasma collagen pull downs. The type III/I collagen receptor, ADGRG1/GPR56, was found to be present on the surface of human platelets. Human platelets and red blood cells (RBCs) isolated from whole-blood samples were stained with antibodies that recognize the GPR56 NTF, the platelet surface marker CD41 (integrin α2b), or the RBC surface marker CD235 (glycophorin A), and relative levels of the markers were measured by flow cytometry. Human platelets, but not the RBCs, stained positive for GPR56 and CD41, whereas RBCs stained positive for CD235 but not GPR56 (Fig. 2*A*). There was variability of GPR56 abundance among platelets isolated from the different human donors (*SI Appendix*, Fig. S2*A*). Intact platelets were costained with the GPR56 NTF antibody and fluorescein isothiocyanate (FITC)-phalloidin and visualized by fluorescent microscopy. Inclusion of the GPR56 rNTF during the antibody incubation blocked the punctate cell surface GPR56 NTF antibody signal (Fig. 2*B*). Cytosol-free membrane homogenates were prepared from human platelets obtained from five donors. The membranes were quantitatively immunoblotted with an antibody to detect the GPR56 CTF (Fig. 2*C*). GPR56 was present in each platelet membrane preparation, and variable abundance was observed, coinciding with the flow cytometry results. The platelet membrane preparations were then treated with urea to dissociate the GPR56 CTF and NTF. The majority of platelet GPR56 was deemed to be self-cleaved as the transmembrane intercalated CTF was resistant to urea solubilization, whereas the majority of the peripherally membrane-associated NTF was urea solubilized

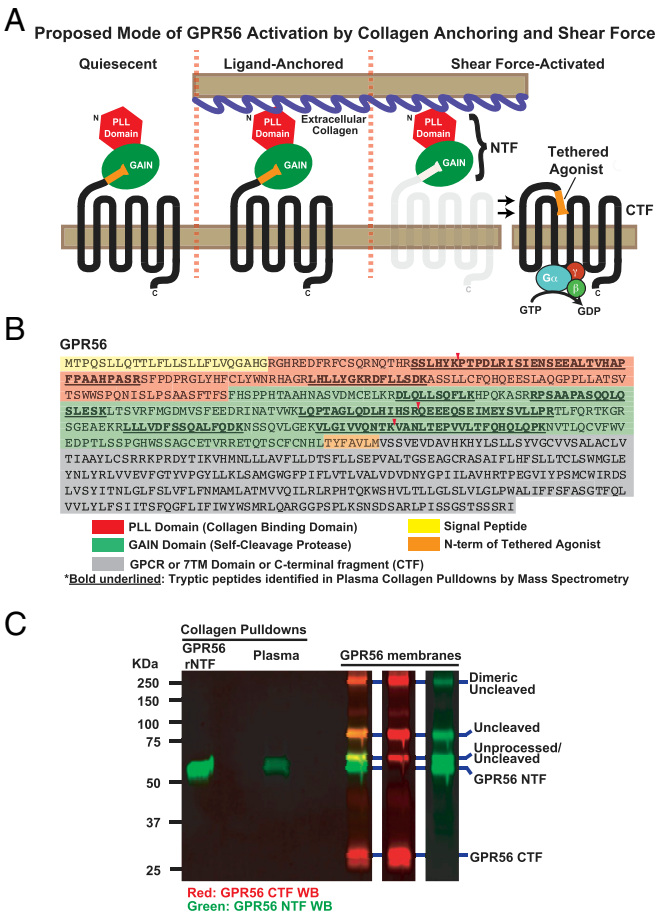

Fig. 1. Identification of the collagen-interacting ADGRG1/GPR56 NTF in human plasma. (*A*) GPR56/ADGRG1 schematic with its N-terminal collagen-binding PLL domain and proposed cell movement, force-mediated, tethered agonism activation mechanism. (*B*) Mass spectrometry tryptic peptide coverage of collagen bead-isolated GPR56 NTF from human plasma. (*C*) GPR56 NTF from human plasma alongside purified GPR56 rNTF was subjected to collagen-coated bead pull down. Eluted proteins and *Sf*9 membranes expressing GPR56 were coimmunoblotted with antibodies to detect the GPR56 NTF and CTF. The eluted proteins and *Sf*9 membranes expressing GPR56 were coimmunoblotted with antibodies to detect the GPR56 NTF (green) and CTF (red). GAIN, G protein-coupled receptor autoproteolysis-inducing domain; 7TM, seven-transmembrane spanning domain.

(Fig. 2*D*). These results demonstrate that the majority of platelet GPR56 is poised for forced-mediated fragment dissociation and activation.

GPR56 activates G12/13 signaling pathways (20–23, 29). Human GPR56 coupled to Gi in vitro and was purported to coimmunoprecipitate Gαq from cells (23, 31). All three of these G protein signaling pathways positively influence the platelet activation program. G13 signaling stimulates Rho-dependent platelet shape changes; Gi inhibits cyclic adenosine monophosphate (cAMP) signaling to promote platelet activation; and Gq stimulus provokes Ca^{+2} release, which reinforces secretion of paracrine and autocrine platelet agonists (2, 32). We closely examined the abilities of human and mouse GPR56 to activate G13 and Gi using receptor membrane reconstitution assays. The GPR56 variant consisting of 687 amino acids was chosen for study as it has much higher basal activity than the longer 693-amino acid variant (*SI Appendix*, Fig. S3) (30, 33). Mouse and human GPR56 robustly activated G13, but only human GPR56 activated Gi (*SI Appendix*, Fig. S4).

We evaluated the ability of endogenous GPR56 to activate downstream signaling pathways controlled by G13 and Gi in isolated human and mouse platelets. GPR56 pharmacological tools were used in the Rhotekin Rho-GTP pull-down assay to assess the influence of platelet GPR56 toward G13-stimulated Rho-GTP production. A *Gpr56*$^{-/-}$ mouse was created for this study (*SI Appendix*, Fig. S5). *Gpr56*$^{-/-}$ and wild-type platelets were harvested from mice, washed, and acutely stimulated with a GPR56 synthetic activating peptide (56-AP), the small molecule GPR56 partial agonist 3-α-acetoxydihydrodeoxygedunin (3-α-DOG), or the synthetic peptide agonist for the Protease Activated 4 Receptor (PAR4-AP) (27, 34). PAR4-AP stimulated Rho-GTP production in wild-type and *Gpr56*$^{-/-}$ platelets, whereas the two GPR56 activators only stimulated Rho-GTP production in wild-type platelets (Fig. 2*E*). Washed human platelets were then stimulated with 56-AP or 3-α-DOG in the presence or absence of a small molecule GPR56 antagonist, dihydromunduletone (DHM) (27, 34). Both GPR56 agonists stimulated rapid Rho-GTP production that was blunted by the DHM antagonist treatment (Fig. 2*F*).

To our knowledge, GPR56 coupling to Gi has not been demonstrated in cells or in tissue, so we tested the ability of GPR56 and the Gi-coupled platelet purinergic receptor ($P2Y_{12}$) agonist, adenosine diphosphate (ADP), to inhibit prostacyclin (PGI_2) and forskolin costimulated cAMP production in isolated human platelets. Forskolin and PGI_2-stimulated Gs synergized to provide robust cAMP production that was inhibited comparably by 56-AP or ADP (Fig. 2*G*). Our past analyses found no evidence that GPR56 could activate Gq in vitro (23); nonetheless, we compared the abilities of 56-AP and PAR4-AP to provoke Gq/11-stimulated Ca^{+2} mobilization in washed human platelets. PAR4-AP elicited a strong Ca^{+2} response, whereas 56-AP had no effect (Fig. 2*H*). These results show that GPR56 provides robust activation of platelet G12/13 signaling, moderate activation of human platelet Gi signaling, and no stimulation of Gq signaling.

GPR56 Stimulates Ex Vivo Platelet Aggregation and Integrin Activation. Turbid suspensions of isolated human platelets aggregate in response to platelet agonists, which include select GPCR agonists and collagen (35). Since GPR56 stimulated platelet G protein signaling, we tested its ability to impact the platelet activation program. Human platelets were isolated from fresh, anticoagulant-treated blood, washed, and introduced into the stirred cell of a Chronolog platelet aggregometer. The GPR56 agonists 56-AP and 3-α-DOG stimulated rapid platelet aggregation, whereas a single point mutant 56-AP control peptide did not (Fig. 3*A*). The potency of GPR56 agonists was compared with that of the established platelet agonist PAR4-AP. The rank order of potencies was 56-AP > PAR4-AP > 3-α-DOG ≠ 56-AP mutant (Fig. 3*B*). The GPR56 antagonist, DHM, specifically inhibited 56-AP– and 3-α-DOG–stimulated platelet aggregation but did not affect PAR4-AP action (Fig. 3 *C* and *D*). Collectively, these results demonstrate that pharmacological modulation of platelet GPR56 activity induces the ex vivo platelet activation and aggregation program.

Platelet aggregation and adhesion to collagen in vivo are supported in part by integrin activation, which is thought to be mediated by complex circuitries of intracellular and extracellular signaling events, including a G13 stimulus (1). We compared the abilities of GPR56 and PAR4 stimulation to induce human platelet integrin activation via human alphaIIbeta3, clone PAC-1 antibody staining, a tool that is used to measure the amount of integrin αIIbβ3 in its active conformation (36, 37). 56-AP provided concentration-dependent integrin activation in human platelets that matched the maximal PAR4-AP–induced response (Fig. 3*E*). GPR56 might fulfill the predicted requirement for the GPCR stimulus that activates G13/Gi to provide the "inside-out signaling" component of integrin activation (38).

Human platelets responded to 56-AP via multiple readouts, but because mouse GPR56 only couples to G13, we hypothesized that 56-AP alone would not induce mouse platelet aggregation or αIIbβ3 integrin activation. We first showed that 56-AP was capable of activating mouse GPR56 by overexpressing the receptor in HEK293T cells and measuring concentration-dependent 56-AP stimulation of the serum response element luciferase gene reporter (*SI Appendix*, Fig. S6*A*). GPR56-AP did not induce wild-type mouse platelet aggregation nor integrin activation when compared with robust PAR4-AP responses observed in both assays (*SI Appendix*, Fig. S6 *B* and *C*). The lack of GPR56-stimulated Gi signaling in mouse platelets was demonstrated directly by showing that forskolin- and PGI_2-coinduced cAMP accumulation was suppressed by ADP but not 56-AP (*SI Appendix*, Fig. S6 *D* and *E*), contrasting previous results in which 56-AP inhibited cAMP production in human platelets (Fig. 2*G*). We sought to compensate for the lack of GPR56 Gi signaling in mouse platelets by inducing platelet aggregation in response to 56-AP when combined with ADP purinergic receptor agonism. However, platelets express two purinergic receptors, $P2Y_{12}$ and $P2Y_1$, with the latter providing Gq stimulus that influences shape change and aggregation. Therefore, to exclude the effects of $P2Y_1$, mouse platelets were pretreated with the $P2Y_1$-selective antagonist, 2′-deoxy-N^6-methyl adenosine 3′,5′-diphosphate (MRS2179), for which a concentration response relationship was developed to determine its ability to inhibit ADP-induced platelet aggregation (*SI Appendix*, Fig. S6*F*). Wild-type but not *Gpr56*$^{-/-}$ mouse platelets aggregated efficiently in the presence of MRS2179 (100 μM), 56-AP (10 μM), and ADP (25 μM) (*SI Appendix*, Fig. S6*G*). These results corroborate previous findings that platelet aggregation relies on synergy of multiple G protein signaling outputs (39, 40). Pharmacological stimulation of human platelet GPR56 induced the ex vivo platelet activation and aggregation programs via the ability of the receptor to activate G13 and Gi.

GPR56 Effects on Platelet Secondary Agonist Release. Primary platelet activation encompasses signaling events that lead to the secretion of agonists from granule contents (e.g., ADP, adenosine triphosphate [ATP], serotonin, magnesium, and calcium ions) as well as oxidized lipid products of cyclooxygenase (COX-1) (41). These diffusible agonists provide secondary activation for platelet recruitment into a growing thrombus (42–44). To learn whether GPR56 activation of platelets relies on secondary agonist signaling, we first assessed granule secretion by measuring released ATP levels during 56-AP–induced human platelet aggregation. 56-AP weakly stimulated dense granule release when compared with the robust PAR4-AP response (Fig. 3*F*), effects that may reflect the different G protein coupling profiles of GPR56 and PAR4 (23, 45). Both receptors activate G13, but

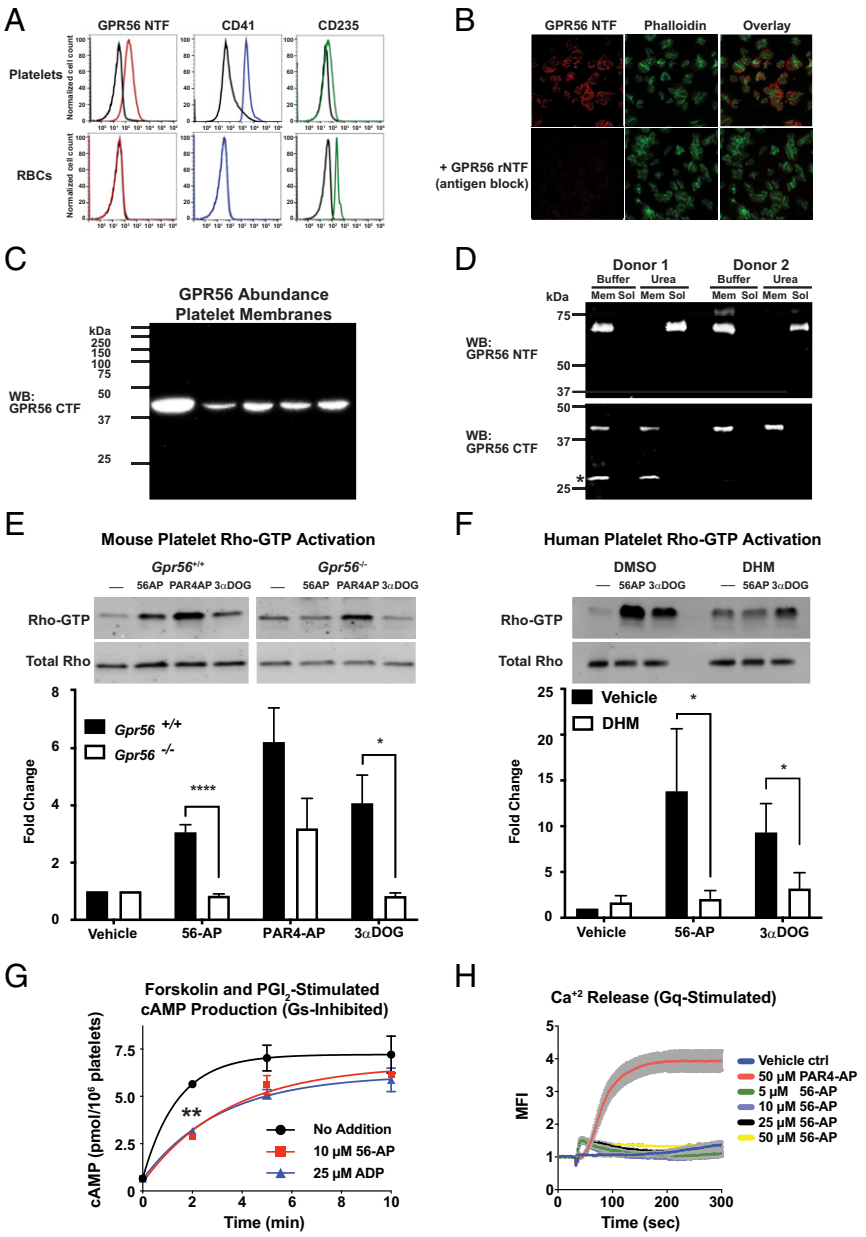

Fig. 2. GPR56 is platelet GPCR that stimulates Rho-GTP production and inhibits cAMP production. (*A*) The GPR56 NTF is present on the surface of human platelets but not RBCs as measured by flow cytometry. Platelets were costained with the platelet marker CD41 or the RBC marker CD235. Representative histogram data from *SI Appendix*, Fig. S2 are shown. (*B*) Intact human platelets were treated with PAR4-AP and adhered and spread on vitronectin-coated glass for 30 min. The intact platelets were costained with the GPR56 NTF antibody (red) and FITC-phalloidin (green) with or without antibody blocking using purified GPR56 rNTF. (*C*) Platelet membranes (20 μg) prepared from five human donors were quantitatively immunoblotted with the GPR56 CTF antisera. (*D*) Platelet membrane GPR56 is predominantly self-cleaved. Two human platelet membrane preparations were mock treated (PBS) or urea treated, and the membrane and solubilized material were immunoblotted for the presence of the GPR56 NTF and CTF. The GPR56 CTF retains membrane association, whereas the NTF was solubilized with urea. *Denotes an alternative SDS/PAGE form of the GPR56 CTF (23). (*E*) Wild-type or $Gpr56^{-/-}$ mouse platelet Rho activation stimulated by 56-AP agonist peptide or 3-α-DOG. Relative total Rho and Rho-GTP levels were quantified by pixel densitometry. Error bars are the mean ± SEM: wild type, $n = 4$; $Gpr56^{-/-}$, $n = 3$. One-way ANOVA. *$P \leq 0.01$; ****$P \leq 0.0001$. (*F*) Human platelet Rho activation stimulated by 56-AP agonist peptide or 3-α-DOG, with or without DHM inhibition. Relative total Rho and Rho-GTP levels were quantified by pixel densitometry. Error bars are the mean ± SEM: human, $n = 4$. One-way ANOVA. *$P \leq 0.01$. (*G*) Forskolin and PGI_2 costimulation of cAMP accumulation in human platelets is inhibited by 56-AP agonist peptide (10 μM) or the purinergic agonist, ADP (25 μM). Error bars are the mean ± SEM ($n = 4$). One-way ANOVA. **$P \leq 0.01$. (*H*) GPR56 activation does not stimulate Gq-mediated calcium release from intracellular stores. Human platelets were treated with 1 mM probenecid and loaded with Fluo4-AM, prior to stimulation with PAR4-AP (50 μM) or 56-AP (concentration series). Shown are the mean fluorescence intensities (MFIs) of intracellular calcium release. Error is the mean ± SEM: $n = 4$. Mem, membrane; Sol, soluble; WB, Western blot.

PAR4 alone activates Gq, which coincides with its ability to strongly induce Ca^{+2}-dependent granule secretion. We next evaluated inhibition of GPR56-AP– and PAR4-AP–induced human platelet aggregation by ADP and the arachidonic acid metabolite, thromboxane A_2 (TXA_2). Human platelets were pretreated with the COX-1 inhibitor, acetylsalicylic acid (ASA), to block platelet TXA_2 generation or with 2-methyl-thio-AMP (2-MeSAMP) to antagonize ADP stimulation of $P2Y_{12}$ (*SI Appendix*, Fig. S7). ASA or 2-MeSAMP alone partially blocked GPR56-AP–induced platelet aggregation but worked additively to provide a strong

block. In contrast, 2-MeSAMP, but not ASA, inhibited PAR4-AP induction of platelet aggregation. These results align with the demonstration of weak granule secretion (e.g., ADP) exerted by GPR56-AP (Fig. 3*F*). Since GPR56 does not couple to Gq, TXA_2 activation of the thromboxane prostanoid receptor TPα, which couples to both Gq and G13, may be required for efficient GPR56-induced platelet aggregation. Direct PAR4 Gq coupling may obviate the requirement for TXA_2 secondary agonism.

GPR56 Stimulates Platelet Shape Change and Spreading. One of the first events of hemostasis is the collagen-stimulated, autonomous conversion of a few circulating discoid-shaped platelets into spheres with filopodia protrusions (1). We first evaluated the GPR56 agonist-induced shape change phase of platelet activation using ex vivo platelet aggregometry experiments in which initial platelet shape changes are realized as a small transient decrease in light transmittance followed by a rapid increased light transmittance phase as platelets aggregate (Fig. 4*A*). We tested the ability of GPR56 agonists and the platelet agonists PAR4-AP and ADP to induce shape change in the presence of L-arginylglycyl-L-α-aspartyl-L-serine (RGDS) synthetic peptide and 2-MeSAMP, platelet inhibitors that blunt the aggregation phase through inhibition of integrin and purinergic receptor Gi stimulus, respectively. PAR4-AP activates Gq/13 signaling, and in this experiment, ADP only activates Gq signaling, due to the 2-MeSAMP inhibition of $P2Y_{12}$ receptor Gi stimulus. Therefore, platelet shape changes are contributed predominantly by G13 signaling with lesser contributions of PAR4 Gq stimulus and GPR56 Gi stimulus. Both GPR56 agonists and PAR4-AP strongly induced platelet shape change (Fig. 4*B*). ADP had no ability to mediate platelet shape change due to 2-MeSAMP inhibition. These results provide a demonstration that GPR56 G protein signaling is sufficient to induce platelet shape change.

The platelet spreading assay is a complimentary measure of shape change. Platelets in dilute suspension will adhere to extracellular matrix-coated surfaces, undergo shape changes and filopodia protrusion, and then flatten or spread. We chose an extracellular matrix that is inert to platelets, vitronectin-coated glass, to evaluate GPR56-induced platelet spreading. The specificity of GPR56 agonists was first evaluated in spreading assays using platelets harvested from wild-type or *Gpr56*$^{-/-}$ mice. GPR56-AP induced spreading of wild-type platelets but not of *Gpr56*$^{-/-}$ platelets, whereas the control, mutant GPR56-AP, had no ability to induce spreading of either wild-type or *Gpr56*$^{-/-}$ platelets (Fig. 4*C*). PAR4-AP stimulated spreading of wild-type and *Gpr56* knockout platelets equally well, showing that the absence of GPR56 did not abrogate the overall ability of platelets to be activated. PAR4-AP and 56-AP induced full, comparable levels of human platelet spreading, whereas 3-α-DOG provided only a moderate level of spreading (Fig. 4*D*). The 56-AP mutant peptide induced no significant human platelet spreading. Fig. 4*E* shows time-lapse images of representative platelet shape change progression induced by GPR56-AP. Filopodia spikes were observed within 2 min of agonist application. The filopodia extended over time, and within 15 min, platelets had begun to spread, and they were fully flattened and firmly adhered at 30 min.

GPR56 Is Required for Efficient Platelet Plug Formation, Hemostasis, and Thrombosis. The *Gpr56*$^{-/-}$ mice were evaluated for hemostatic defects using a tail injury bleeding assay (46, 47). *Gpr56*$^{-/-}$ mice exhibited a pronounced hemostasis defect in that the majority of knockout mice had prolonged times to bleeding cessation, with approximately one-quarter of the cohort requiring cauterization (Fig. 5*A*). Recording of instances of temporary bleeding stoppage, resumption, and final cessation showed that 73% of *Gpr56*$^{-/-}$ mice (16/22) exhibited rebleeding events, whereas only 21% (4/19) of *Gpr56*$^{+/-}$ and 7% (1/15) of *Gpr56*$^{+/+}$ mice did (Fig. 5*B*). These data indicate that prolonged bleeding in *Gpr56*$^{-/-}$ mice may be attributed to unstable clot formation.

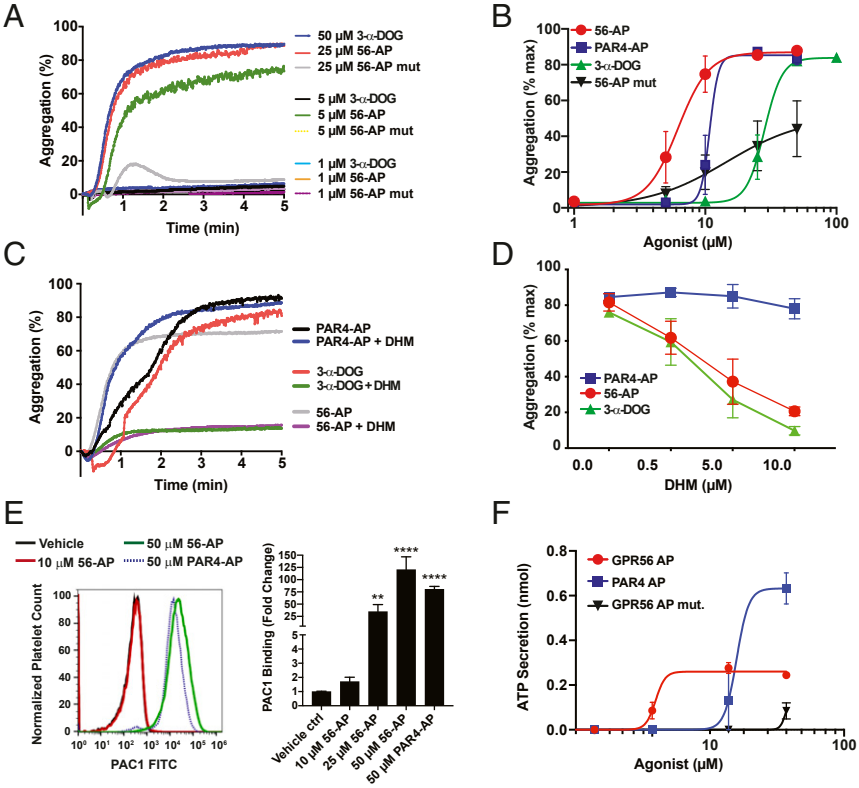

Fig. 3. GPR56 activates platelet aggregation and integrin activation. (*A*) Representative tracings of human platelet aggregation in response GPR56 peptide agonist mimetics (56-AP and 56-AP mutant) and 3-α-DOG. (*B*) Concentration response curves of human platelet aggregation mediated by 56-AP, 56-AP mutant, PAR4-AP, and 3-α-DOG. Error bars are the mean ± SEM ($n = 5$). (*C*) Representative aggregometry tracings of 56-AP–, 3-α-DOG–, and PAR4-AP–induced human platelet aggregation at 80% maximal effective concentration (EC_{80}) with DHM inhibition. (*D*) Concentration response curves of DHM inhibition of human platelet aggregation induced by GPR56, 3-α-DOG, and PAR4 agonists at EC_{80}. Error bars are the mean ± SEM ($n = 5$). (*E*) Flow cytometric analysis of αIIbβ3 integrin activation via PAC-1–FITC staining of human platelets treated with a 56-AP concentration series or a maximal PAR4-AP concentration. Representative mean fluorescent intensity traces of PAC-1–FITC binding to human platelets are shown alongside histograms. Error bars are the mean ± SEM ($n = 6$). One-way ANOVA. $^{**}P \leq 0.01$; $^{****}P \leq 0.0001$. (*F*) Concentration response relationships of 56-AP, 56-AP mutant, and PAR4-AP toward ATP secretion as measured in a Lumi-aggregometer. Error bars are the mean ± SEM ($n = 5$).

Hemostatic platelet plug formation in the cremaster arterioles of live mice was examined using a vessel wall laser injury assay. Video microscopy monitored the progression of platelet plug formation after injury via the accumulation of Alexa-Fluor 488-conjugated anti-GPIbβ (platelets) and fibrin deposition through Alexa-Fluor 647-conjugated antifibrin accumulation. *Gpr56*$^{-/-}$ mice formed platelet plugs that were dramatically reduced in size in comparison with wild-type mice (Fig. 5 *C* and *D* and Movie S1). Qualitative inspection of the movies showed increased instances of emboli release from the growing plugs in *Gpr56*$^{-/-}$ mice, which is consistent with an unstable clotting phenotype. Levels of fibrin deposition at the injury sites were equivalent in *Gpr56*$^{-/-}$ and wild-type mice (Fig. 5*E*). A low platelet count is one potential explanation for reduced platelet plug formation, yet no significant differences were observed in platelet counts when total blood counts of wild-type and *Gpr56*$^{-/-}$ mice were compared (*SI Appendix*, Table S2). From these results, we propose that *Gpr56*$^{-/-}$ platelets do not readily accumulate at sites of vessel wall injury because they are defective in undergoing the shape changes and integrin activation that precede firm platelet adhesion.

We injected GPR56 rNTF into mouse circulation to test whether it could inhibit platelet interactions with collagen via hemostasis readouts. GPR56 rNTF-injected mice had substantially prolonged times to bleeding cessation in the tail injury assay compared with the vehicle-injected group (Fig. 5*F*). The GPR56 rNTF was preinjected into wild-type mice prior to laser-induced injury of the cremaster arteriole. GPR56 rNTF-injected mice developed hemostatic plugs that were substantially reduced in size in comparison with vehicle-injected mice (Fig. 5 *G* and *H* and Movie S2). Interestingly, the GPR56 rNTF-injected mice also had substantially reduced levels of fibrin accumulation at injury sites (Fig. 5*I*). This result is interesting when considering the findings of Fig. 5*E* that showed that accumulated fibrin levels were equivalent in wild-type and *Gpr56*$^{-/-}$ mice. This indicates that GPR56 rNTF not only may block endogenous platelet GPR56 interaction with injury-exposed subendothelial collagen but may block collagen interactions with other hemostatic factors, including fibrin.

The cremaster arteriole injury model represents a view of platelet plug formation in microcirculation. We tested the requirement of GPR56 in a large vessel model of induced thrombotic occlusion. Platelets harvested from *Gpr56*$^{-/-}$ and wild-type mice were labeled with calcein-acetoxymethyl (calcein-AM) dye and injected into circulation of genetically identical recipient mice. Recipient mouse carotid arteries were surgically prepared for intravital microscopy and denuded by application of $FeCl_3$ to injure the vessel walls prior to the start of the video recordings. Both cohorts reached full vessel occlusion, but *Gpr56*$^{-/-}$ mice exhibited significant delays (Fig. 6 and Movie S3). The cause of the delay appeared to be due to the instability of *Gpr56*$^{-/-}$ platelet plugs, as more emboli were observed in this group. Collectively, our results demonstrate that GPR56 is required for efficient hemostasis and thrombosis in both microcirculation and large vessels.

GPR56 Is Required for Shear Force-Dependent Platelet Adhesion to Collagen. To arrive at a mechanism of GPR56 action in hemostasis, we tested the codependence of GPR56 and shear force for ex vivo platelet adhesion to immobilized, equine tissue collagen. Whole blood from *Gpr56*$^{-/-}$, *Gpr56*$^{+/-}$, or *Gpr56*$^{+/+}$ mice was treated with the platelet permeable dye 3,3′-dihexyloxacarbocyanine Iodide (DiOC6) and perfused through collagen-coated microflow chambers at a high shear rate (1,800 s^{-1}) to mimic the force experienced by cells and platelets in arterioles and at a lower shear rate (400 s^{-1}) to mimic venous shear force. Time-lapse video microscopy monitored platelet adherence onto collagen. At high shear force, *Gpr56*$^{-/-}$ platelets had a dramatic defect in adhering to the immobilized collagen (Fig. 7 *A* and *B* and Movie S4). *Gpr56*$^{+/-}$ exhibited modest adhesion impairment in comparison with wild-type platelets. In contrast, there were no differences among *Gpr56*$^{-/-}$, *Gpr56*$^{+/-}$, and *Gpr56*$^{+/+}$ platelets in adherence to the collagen at low shear force (Fig. 7 *C* and *D* and Movie S5), indicating that the complement of other adhesive collagen receptors present on platelets was sufficient to mediate platelet adhesion at low shear in the absence of GPR56. Although *Gpr56*$^{-/-}$ platelets were defective in adhering to collagen at high shear, we observed no defects of these platelets in ex vivo aggregation assays when stimulated by collagen or PAR4-AP. (*SI Appendix*, Fig. S8). This may be due to the performance of light transmission aggregometry (LTA) under nonphysiological parameters, as platelets are induced to form aggregates under low shear rates (<100 s^{-1}) (48, 49). Collagen-induced platelet aggregometry may not fully simulate all of the events of platelet adhesion and activation that are induced in vivo by insoluble collagen that is exposed upon vessel wall damage (50). At the high shear rate, we propose that GPR56 induces collagen-dependent platelet filopodia protrusion and shape change that permit other platelet adhesive collagen receptors to promote stable platelet adhesion.

Given that GPR56 rNTF exhibited strong anticoagulant action when injected into mice (Fig. 5 *F*–*I*), we next tested its ability to inhibit platelet adhesion to immobilized collagen. Whole human blood supplemented with GPR56 rNTF or vehicle was perfused through the collagen-coated microflow chambers at the high shear rate. Platelets from GPR56 rNTF-treated blood adhered dramatically less well than those from vehicle-treated blood (Fig. 7 *E* and *F* and Movie S6). We surmise that the compilation of GPR56 rNTF anticoagulant and hemostatic effects is manifested by it blocking available collagen-binding sites for platelet GPR56, other platelet collagen receptors, and for fibrin deposition.

Discussion

Our work demonstrates that GPR56 is an initial responder to collagen and serves to transduce blood flow-induced shear force to activate G13-stimulated platelet shape change and integrin activation. In our working model, GPR56 may work immediately after platelet tethering and then in concert with GP1b-IX-V/vWF-bound collagen (Fig. 8). Circulating platelets are captured and decelerated via GPIb binding to vWF-associated collagen (5, 51). They roll along collagen through a series of formed and broken GP1b/vWF interactions (2, 9, 10, 52, 53). We propose that there is a simultaneous interaction of the GPR56 PLL domain with the mixed collagen matrix, and the force created by platelet rolling dissociates the extracellular NTF from the platelet membrane-associated CTF. The GPR56 CTF is then rapidly activated by first-order binding of its tethered peptide agonist, resulting in rapid G13 signaling and induction of the actin cytoskeletal arrangements that facilitate platelet shape change. Platelet filopodia protrusions that arise due to G13 signaling act to slow the platelet further and allow adhesive platelet collagen receptors to induce spreading, firm adhesion, and platelet plug formation. A potential consequence of this proposed mode of platelet GPR56 activation is that the NTF is jettisoned onto the collagen. Due to continuous blood flow, the collagen-deposited NTF may eventually be liberated into the blood plasma for clearance. In Fig. 1*B*, collagen-coated beads were used to isolate the GPR56 NTF from clarified plasma. No GPR56 CTF was found attached to the beads, indicating that the origin of the plasma GPR56 NTF population was likely from a cell that was exposed to circulation and had experienced shear force. There are a number of potential sources of GPR56 among circulating cells. In addition to platelets (Fig. 2 *A*–*D*), GPR56 is present on hematopoietic stem cells and select circulating immune cells, including natural killer (NK) cells and lymphocytes (54–56). We know of no evidence demonstrating the presence of GPR56 on endothelial cell types that line vessel walls. An active area of future investigation will be to discern if the major source of plasma GPR56 NTF is derived from the circulating platelets and whether GPR56 NTF levels in plasma might be prognostic of thrombotic events (57).

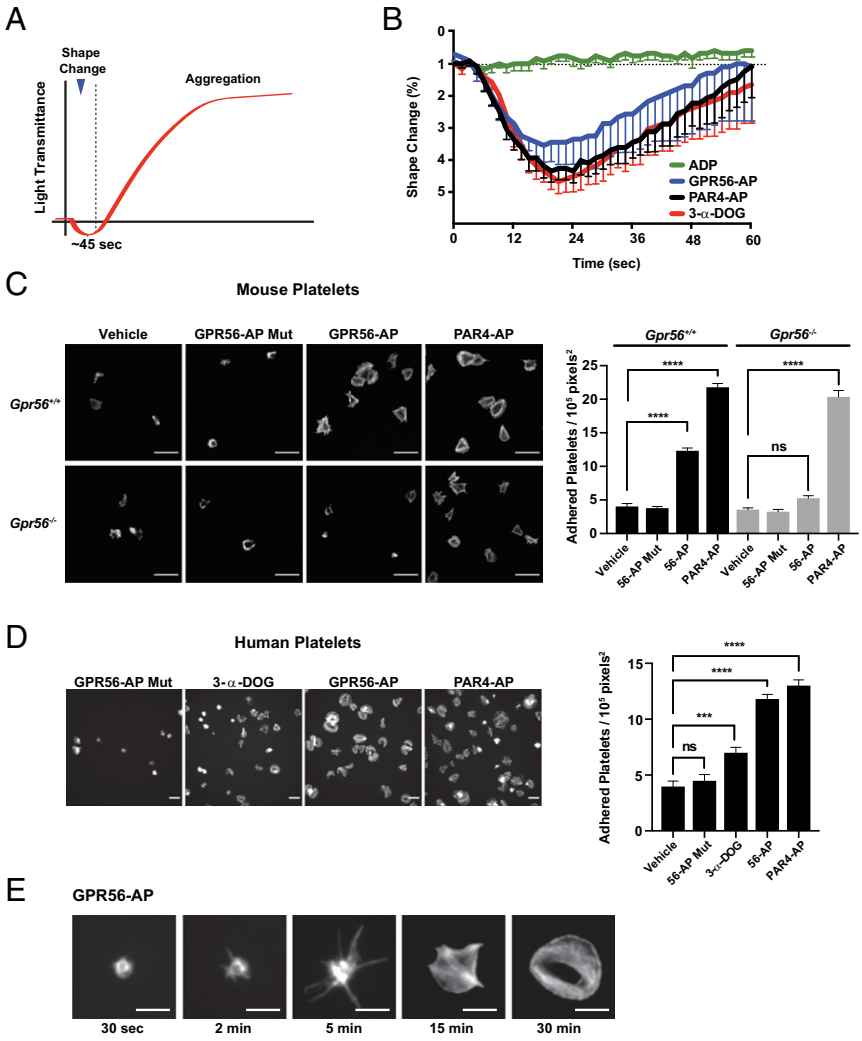

Fig. 4. GPR56 induces platelet shape change, filopodia extension, and spreading. (*A*) Schematic showing idealized light transmittance phases of shape change and aggregation of agonist-treated platelet suspensions. (*B*) GPR56 agonists (GPR56-AP and 3-α-DOG) and PAR4-AP induce platelet shape change in the presence of integrin and purinergic receptor inhibitors (RGDS synthetic peptide and 2-MeSAMP). Values are mean ± SEM. (*C*) *Gpr56*$^{+/+}$ and *Gpr56*$^{-/-}$ mouse platelet spreading onto vitronectin-coated glass in response to GPR56-AP, GPR56-AP mutant, and PAR4-AP. Shown are representative fields of phalloidin-stained platelets at 100× magnification. Quantification is adhered platelets per unit area (10^5 pixels^2, $n = 15$). Values are mean ± SEM. One-way ANOVA. ****$P \leq 0.0001$. (Scale bar, 10 μm.) (*D*) Human platelet spreading onto vitronectin-coated glass in response to GPR56-AP, GPR56-AP mutant, 3-α-DOG, and PAR4-AP. Shown are representative fields of phalloidin-stained platelets at 100× magnification. Quantification is adhered platelets per unit area (10^5 pixels^2, $n = 15$). Values are mean ± SEM. One-way ANOVA. ***$P \leq 0.001$; ****$P \leq 0.0001$. (Scale bar, 10 μm.) (*E*) Time course of human platelet spreading onto vitronectin-coated glass in response to GPR56-AP. Representative images of phalloidin-stained platelets are from $n = 4$ experiments and show progressive filopodia protrusion, lamellipodia formation, and spreading. (Scale bar, 5 μm.) ns, nonsignificant.

It is well established that G13 signaling is required to induce platelet shape changes in response to thrombin (18, 19). Collagen-induced activation of G13 for platelet shape change and integrin activation are not readily explained by the action of the current repertoire of platelet collagen receptors, none of which are GPCRs. The timing of the proposed signaling routes of collagen-induced platelet shape change are protracted and do not adequately explain the rapidity of the in vivo process. The first platelet collagen receptor or vWF/collagen receptor, GP1b-IX-V, provides a miniscule Ca^{+2} signaling output (58–64). A second platelet collagen receptor, GPVI/FcRγ, stimulates a tyrosine kinase cascade that was proposed to be the key inducer of integrin $\alpha_2\beta_1$ activation for mediation of firm platelet adhesion and aggregation (5, 13, 65–67). GPVI/FcR γ kinase signaling results in the assembly of a large adaptor protein complex that is important for PLCγ2 activation. Within the kinase cascade, multiple scaffold proteins and kinases are involved, leading to eventual calcium release from intracellular stores, granule secretion, and thromboxane production to promote inside-out signaling and integrin activation. The timing of these signaling events may not fully account for or reflect the immediate, primary platelet response that is required to trigger pronounced shape change morphology (68, 69). A previous model describing the interplay of GPVI and integrin function indicated a potential for an undescribed GPCR stimulus of the G13 signaling (38). Our work indicates that GPR56 fulfills this role while working with the established glycoprotein receptors during platelet transient adhesion to collagen.

Our work has also provided evidence that further supports a model of AGPCR NTF/CTF dissociation-mediated activation. GPR56 has a number of described extracellular matrix protein ligands, of which the best characterized is type III collagen (21, 29, 70–72). Type I collagen was also obtained as a ligand in the original GPR56 deorphanization work (21). Types I and III collagen are the major collagen subtypes present in the subendothelial layers surrounding vessel walls (73, 74). AGPCR protein ligands bind to adhesive modules within the NTFs. It has been proposed that the ligand–NTF interaction serves the purpose of anchoring the NTF; in the case of platelet GPR56, this is to the collagen that becomes exposed after vessel wall injury. In our study, we observed GPR56 and shear-force dependence of platelet adhesion to immobilized collagen (Fig. 7 *A*–*C*). Moreover, the detection of free GPR56 NTF in blood plasma coincides with these findings. Our current work is focused on detecting freed GPR56 NTF bound to collagen in the hemostasis models; however, these experiments are complicated by the massive recruitment of platelets that contain substantial GPR56, which interferes with the ability to distinguish the free from collagen-bound GPR56 NTF.

Our delineation of differential G protein coupling of human and mouse GPR56 may help to explain some longstanding observational differences of human and mouse platelet performance in standardized assays. Wild-type mouse platelets spread

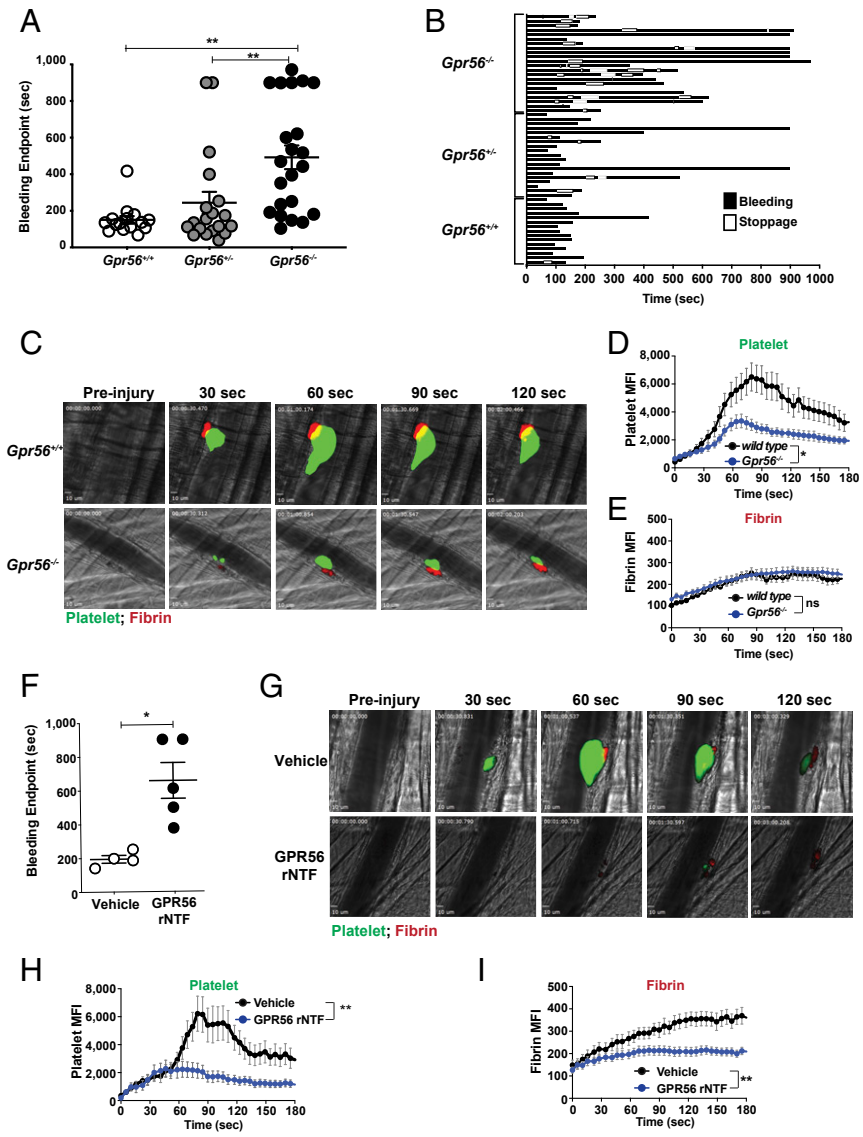

Fig. 5. GPR56 is required for efficient hemostasis and platelet plug formation. Mouse tail injury bleeding assay results are reported (*A*) as times to final bleeding cessation and (*B*) in detail to show instances of temporary bleeding, stoppage, and resumption. (*C–E*) Mouse cremaster arteriole laser-induced injury assay showing representative platelet plug formation (green platelets) and fibrin accumulation (red). The still images accompany Movie S1. Quantification of mean fluorescence intensity (MFI) of platelet accumulation or fibrin accumulation. Error bars are the mean ± SEM (n = 30 and 28 injuries among three $Gpr56^{+/+}$ or $Gpr56^{-/-}$ mice, respectively). (*F*) Mouse tail injury bleeding assay of wild-type mice injected with vehicle or an equivalent volume of purified GPR56 rNTF protein (5 mg/kg). (*G*) Mouse cremaster arteriole laser-induced injury assay showing representative platelet plug formation and fibrin accumulation in wild-type mice injected with vehicle or purified GPR56 rNTF protein (5 mg/kg). The still images accompany Movie S2. (*H* and *I*) Quantification of MFI of platelet accumulation and fibrin accumulation. Error bars are the mean ± SEM (n = 13 injuries among two mice injected with vehicle and n = 21 injuries among three mice injected with GPR56 rNTF). *P < 0.05, **P < 0.005; ns, nonsignificant.

efficiently on an inert matrix in response to GPR56-AP (Fig. 4); however, GPR56-AP did not induce mouse platelet aggregation nor integrin activation (*SI Appendix*, Fig. S6 *A* and *B*), in contrast to human platelets that did spread and aggregate (Fig. 3 *A* and *B*). Human GPR56 couples to G13 and Gi, whereas mouse GPR56 only couples to G13 (*SI Appendix*, Figs. S3 and S4). This aligns with previous reports that G13 signaling alone is not sufficient for platelet aggregation but requires both Gi and G13 signaling for efficient integrin activation to mediate platelet aggregation (39, 40) (*SI Appendix*, Fig. S7).

As GPR56 is a collagen receptor, our initial hypothesis was that $Gpr56^{-/-}$ mouse platelets would not respond to collagen in vitro. Conversely, $Gpr56^{-/-}$ platelets aggregated normally in response to collagen during LTA (*SI Appendix*, Fig. S8 *A* and *B*). During LTA, washed platelets in the stirred suspension experience less than 100 s^{-1} of shear force, and the collagen is not immobilized (48, 49). LTA does not fully mimic the conditions that platelets experience in vivo, including high shear force and interactions with the damaged vessel wall and underlying extracellular matrix. Our mechanistic model requires shear force and anchoring of the GPR56 NTF to collagen. Therefore, our results for GPR56 align with previous observations from multiple mouse models in which clear hemostatic defects were observed in vivo, but normal platelet aggregation or integrin activation was observed in vitro. For example, the chimeric IL4Rα/GPIbα-*tg* mouse model produces a GP1b protein that lacks its collagen-binding site and therefore, recapitulates features of the bleeding disorder Bernard–Soulier syndrome (75). These mice have reduced thrombus growth, delayed mesenteric artery occlusion, and abolished platelet adhesion to sites of vessel injury (76). Despite these clear in vivo defects, isolated IL4Rα/GPIbα-tg platelets aggregated normally in response to the platelet agonists, ADP, thrombin, and collagen (77).

We have found no evidence from genome-wide association studies that have indicated a role for GPR56 in hemostasis. This may be due to the fact that GPR56 is expressed broadly in tissues ranging from skeletal muscle, NK cells, pancreatic β cells, and the brain, indicating that GPR56 undoubtedly has pleotropic function (54, 72, 78–80). Therefore, future experiments will be directed to examine hemostatic defects in mice with conditional deletion of *Gpr56* in platelets or in the lineage from which platelets arise. In the brain, GPR56 reduction-of-function mutations cause the embryonic-originated, recessive cortical malformation disease bilateral frontoparietal polymicrogyria (BFPP) (81, 82). Mice with *Gpr56* null mutations live normal life spans while recapitulating many features of the human BFPP disorder, yet until now, a

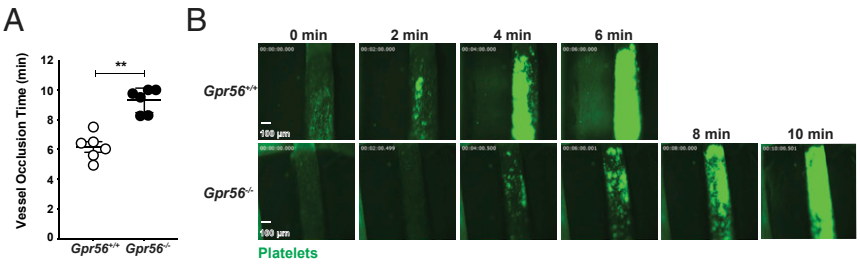

Fig. 6. Mice lacking GPR56 are delayed in forming occlusive thrombi in the carotid artery. (*A*) Mouse carotid artery $FeCl_3$-induced thrombosis assay showing times to reach full vessel occlusion in genetically identical recipient mice injected with calcein-AM–labeled *Gpr56*$^{+/+}$ or *Gpr56*$^{-/-}$ donor platelets. Error bars are the mean ± SEM ($n = 6$). (*B*) Representative still images showing progression to full vessel occlusion that accompany Movie S3. $^{**}P < 0.005$.

hemostasis defect was not noted in these mice. It will be interesting to carefully examine BFPP patients for potential hemostasis defects.

There is potential opportunity to develop new classes of pro- or anticoagulant therapeutics based on GPR56 signaling or its interaction with collagen. Administration of the GPR56 rNTF to wild-type mice elicited pronounced defects in hemostasis. GPR56 rNTF-treated mice had significantly prolonged tail bleeding times and reduced thrombus formation (platelet and fibrin accumulation) at sites of vessel wall injury (Fig. 5 *F*–*I*). The reduced fibrin accumulation in the arteriole–hemostatic/thrombosis model (Fig. 5*I*) strongly suggests that the rNTF generally interferes with multiple hemostatic factors, perhaps in a competitive manner. Studies are underway to directly observe rNTF or NTF accumulation at vessel injury sites and to explore the potential that a smaller portion of the GPR56 rNTF might exhibit anticoagulant properties (e.g., the ∼15-kDa PLL, collagen-binding domain). Delineation of the precise GPR56 collagen-binding site will also support development in this area. Ongoing work in the development of small molecule GPR56 agonists and antagonists affords additional opportunity to develop new classes of hemostatic drugs (27, 34).

Materials and Methods

Reagents. The following primary or secondary antibodies were used: normal mouse and goat IgG antibodies (Santa Cruz Biotechnology); FITC anti-human CD235a, FITC anti-human CD41/CD61 (PAC1), and anti-human CD41 (Biolegend); anti-RhoA, GPR56 CTF (EMD Millipore); mouse alphaIIbeta3 antibody clone JON/A-phycoerythrin (PE), anti-GPIb DyLight-488 (Emfret); Alexa-Fluor 488-conjugated phalloidin, Alexa-Fluor 647 donkey anti-sheep IgG, and Alexa-Fluor 488 donkey anti-mouse IgG (ThermoFisher Scientific); 690LT donkey anti-mouse and 800CW donkey anti-rabbit (LI-COR); and GPR56 NTF (R&D Systems). Antifibrin (clone 59D8) was provided by Rodney Camire, Children's Hospital of Philadelphia, Philadelphia, PA. Custom GPR56 peptides GPR56 P7, TYFAVLM-NH_2; GPR56-AP, TYFAVLMQLSPALVPAELL-NH_2; and GPR56-AP Mutant TNFAVLMQLSPALVPAELL-NH_2 were synthesized and high performance liquid chromatography (HPLC) purified by Genscript. PAR4-AP (AYPGKF-NH_2) and RGDS peptide were from GL Biochem and Sigma-Aldrich, respectively. Small molecule compounds 3-α-DOG and DHM were purchased from Microsource Discovery Systems.

Human Subject Recruitment and Platelet Isolation. This study was approved by the University of Michigan Institutional Review Board. Written informed consent was obtained from healthy volunteers prior to blood collection in the Department of Pharmacology Blood Core Facility. Blood was drawn into vacutainers containing sodium citrate for platelet preparation or heparin for microfluidic perfusion flow chamber assay. Citrated blood was centrifuged at 200 × *g* to separate platelet-rich plasma (PRP) from RBCs. PRP was transferred to tubes containing 10% vol/vol acid citrate dextrose solution (ACD) and apyrase (0.02 U/mL) and centrifuged at 2,000 × *g*. The platelet count was adjusted to 3×10^8 platelets per milliliter with Tyrode's buffer for all studies, unless otherwise stated.

Murine Blood Collection, Platelet Isolation, and Complete Blood Counts. The Institutional Animal Care and Use Committees at the University of Michigan approved all experimental procedures involving mice. A colony of C57BL/6 *Gpr56*$^{+/-}$ mice was maintained, and progeny were genotyped according to an established protocol (83). Blood was drawn from the inferior vena cavae of 8- to 12-wk-old anesthetized mice with a 21-gauge needle attached to a 1-mL syringe containing either 20 U of heparin or 100 μL of 3.8% wt/vol sodium citrate. Retroorbital blood was collected into ethylenediaminetetraacetic acid (EDTA)-treated tubes and analyzed with a Hemavet (Drew Scientific) to obtain complete blood counts. Heparinized mouse blood was used immediately in perfusion chamber assays, while citrated mouse blood was used for platelet isolation. Citrated mouse blood was diluted with an equal volume of Tyrode's buffer and centrifuged at 200 × *g*. PRP was transferred to a tube containing a 10% vol/vol ACD solution, prostaglandin E1 (PGE_1) (50 ng/mL; Cayman Chemical), and apyrase (0.02 U/mL; Sigma-Aldrich) and centrifuged at 2,000 × *g*. Platelet counts were adjusted to 3×10^8 platelets per milliliter with Tyrode's buffer for all studies, unless otherwise stated.

Flow Cytometric Measurement of Cell Surface Receptor Levels and Integrin αIIbβ3 Activation. Washed human platelets and RBCs (1.5×10^7) were fixed with 4% wt/vol paraformaldehyde in phosphate buffered saline (PBS) for 15 min, washed three times with PBS, blocked in PBS containing 3% wt/vol bovine serum albumin (BSA) for 1 h, and stained with the following antibodies for 18 h at 4 °C: 1/50 vol/vol GPR56 NTF, FITC anti-mouse CD41, CD235a, or IgG control antibodies (goat or mouse). Cells were washed three times with PBS to remove unbound antibodies, resuspended in PBS, and incubated with 1/1,000 Alexa-Fluor secondary antibodies, Alexa-Fluor 488, or Alexa-Fluor 647 for 1 h. Cells (50,000) were washed three times and resuspended in PBS prior to flow cytometry analysis (BD Accuri C6). For measurement of integrin αIIbβ3 activation, 1.5×10^7 washed human or mouse platelets were resuspended in 1/10 vol/vol FITC-conjugated anti-human PAC-1 or PE-conjugated JON/A in Tyrode's buffer prior to stimulation with the indicated agonists (56-AP or PAR4-AP) for 10 min. Platelets (50,000) were postfixed with 2% wt/vol paraformaldehyde for 15 min, diluted in 500 μL of Tyrode's buffer, and measured in a flow cytometer (BD Accuri C6), and data were analyzed with FlowJo software (BD).

Platelet Membrane Preparation and Immunoblotting. Packed platelets freshly prepared from 60 mL of human blood samples were washed in Tyrode's solution and suspended in 2 mL of 20 mM 4-(2-hydroxyethyl)-1-piperazineethanesulfonic acid (Hepes), pH 7.4, 1 mM ethylene glycol-*bis*(2-aminoethylether)-*N*,*N*,*N*′,*N*′-tetraacetic acid (EGTA), and protease inhibitor mixture (23 μg/mL phenylmethylsulfonyl fluoride, 21 μg/mL Nα-p-tosyl-L-lysine-chloromethyl ketone, 21 μg/mL L-1-*p*-tosylamino-2-phenylethyl-chloro ketone, 3.3 μg/mL leupeptin, 3.3 μg/mL lima bean trypsin inhibitor). Platelets were lysed using a nitrogen cavitation device (Parr Industries). Lysates were centrifuged at 1,000 × *g*, and the supernatant was centrifuged at 100,000 × *g* for 30 min. Cytosol was discarded, and the membrane pellet was washed and suspended in 20 mM Hepes, pH 7.4, 1 mM EGTA, and 12% wt/vol sucrose by Dounce homogenization. The total protein content of each sample was determined by Bradford assay. Membrane homogenate (20 μg) was added to reducing SDS/PAGE sample buffer. Unheated samples were resolved by 12% SDS/PAGE and immunoblotted with the GPR56 CTF and GPR56 NTF antibodies. For urea solubilization experiments, membranes were collected by 100,000 × *g* centrifugation and Dounce homogenized at 4 °C into 20 mM Hepes, pH 7.4, and 1 mM EGTA or 20 mM Hepes, pH 7.4, 1 mM EGTA, and 7 M urea. The insoluble material was separated by 100,000 × *g* centrifugation. Soluble and insoluble samples were subjected to SDS/PAGE and immunoblotting with the GPR56 CTF and NTF antibodies.

Platelet Aggregometry, Platelet Shape Change Analysis, and ATP Secretion. Platelet aggregation and dense granule secretion experiments were simultaneously performed in a Chrono-log Lumi-aggregometer at 37 °C under stirring conditions. Platelets were stimulated with the indicated agonists (56-AP, 3-α-DOG, PAR4-AP, ADP, or collagen), and light transmission of platelet aggregation was monitored at 500-ms intervals for 5 min to determine final or maximal aggregation. Platelet shape change was observed in the presence of integrin and purinergic receptor inhibitors (RGDS synthetic peptide and 2-MeSAMP) before agonist stimulation at 37 °C under stirring conditions. The amount of decrease in light transmittance was recorded for

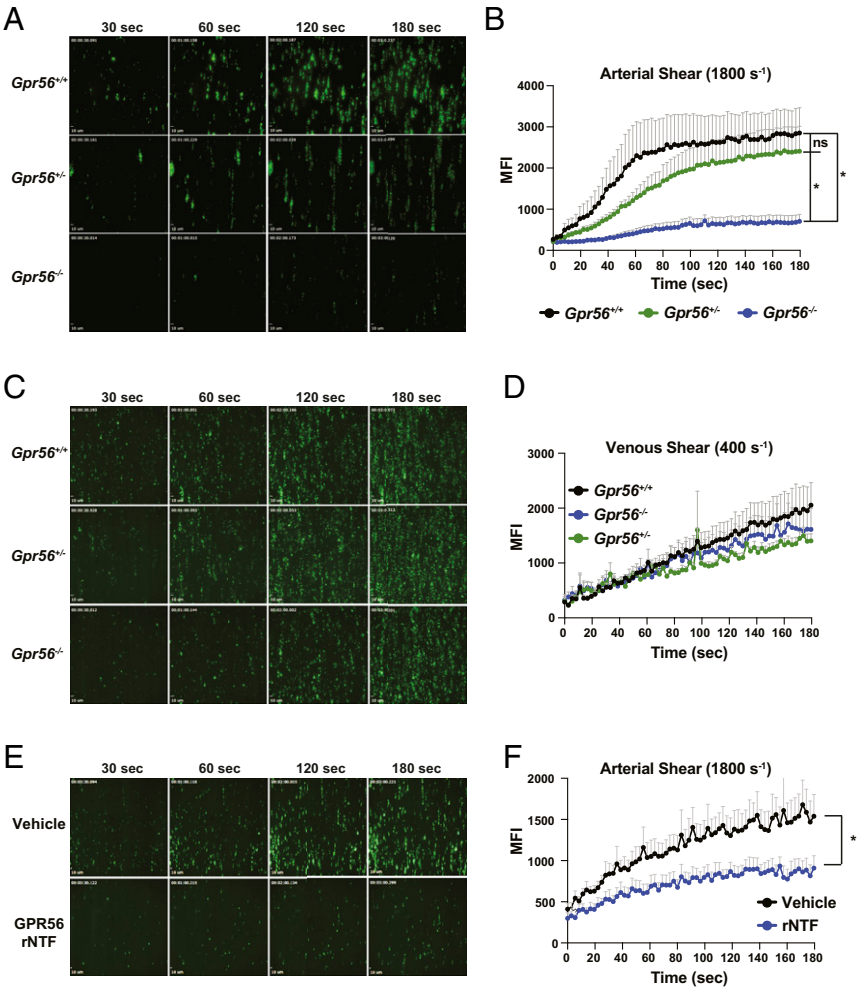

Fig. 7. GPR56 is required for shear force-dependent platelet adhesion to immobilized collagen. *Gpr56*$^{+/+}$, *Gpr56*$^{+/-}$, and *Gpr56*$^{-/-}$ mouse blood was incubated with DiOC6 to stain platelets fluorescently green and was flowed through small bore chambers coated with immobilized collagen at (*A* and *B*) a high shear rate to mimic arterial blood flow-induced shear forces or (*C* and *D*) a low shear rate to mimic typical venous blood flow-induced shear force. Time-dependent platelet adhesion to collagen was monitored by video microscopy. The representative still images accompany Movies S4 (arterial shear) and S5 (venous shear). Mean fluorescence intensity (MFI) of the adhered and aggregated platelet signals. (*E* and *F*) Human blood was treated with DiOC6 and supplemented with vehicle or 250 nM GPR56 rNTF. The blood was flowed over immobilized collagen at a high shear rate (1,800 s^{-1}), and platelet adhesion was monitored by time-lapse video microscopy. The representative still images accompany Movie S6. MFI of the adhered platelet signals. Error bars are the mean ± SEM (n = 5 flow trials for each condition). *$P < 0.05$. ns, nonsignificant.

1 min after agonist stimulation. ATP secretion was measured concurrently using Chrono-Lume (Chronolog), a luciferin/luciferase mixture.

Cremaster Arteriole Laser-Induced Injury Hemostasis Model. Mice were anesthetized by intraperitoneal injection of 100 mg/kg of ketamine/xylazine prior to mounting of cremaster muscle arterioles (30- to 50-μm diameter each) under a dissecting microscope with constant perfusion of bicarbonate-buffered saline at 37 °C (84–86). Antiplatelet (anti-GPIb DyLight 488, 1 μg/g mouse) and antifibrin (Alexa-Fluor 647-conjugated, 0.3 μg/g mouse) were administered via jugular vein catheter prior to intravital microscopy (87, 88). Injuries were induced in the arterioles using a laser ablation system (532-nm laser pulses via the Ablate! photo-ablation system; 3I). Videos of thrombus formation were acquired in real-time using a 63× water-immersion objective with a Zeiss Axio Examiner Z1 fluorescent microscope equipped with solid laser launch system and high-speed scientific complementary metal–oxide–semiconductor (sCMOS) camera. All captured images were analyzed using Slidebook software (3i).

$FeCl_3$-Induced Carotid Artery Injury Thrombosis Model. Mouse *Gpr56*$^{-/-}$ and *Gpr56*$^{+/+}$ platelets were prepared as described above and fluorescently labeled with 1 μM calcein-AM (ThermoFisher Scientific). Calcein-AM–labeled platelets (2×10^6 platelets per gram mouse) were injected via tail vein into genetically identical recipient mice. Recipient mice were anesthetized prior to the surgical exposure of the right common carotid artery (89). Whatman filter paper (1 mm^2) was saturated with a 10% wt/vol solution of $FeCl_3$ and topically placed on the exposed carotid artery for 2 min to initiate thrombosis (90). $FeCl_3$-induced thrombosis progression was recorded in real time using the 5× objective of a Zeiss Axio Examiner Z1 fluorescent microscope until full vessel occlusion was observed. Videos were analyzed using Slidebook software (3i).

Mouse Tail Bleeding Assay. Mice were anesthetized with ketamine/xylazine and placed on a 37 °C heating pad in the prone position. Distal 5-mm sections of the tail were amputated with a sterile scalpel. The amputated tails were immediately immersed into a tube containing 15 mL of 37 °C prewarmed isotonic saline solution (0.9% wt/vol). Bleeding was visually monitored and hand timed. Stoppage and resumption events were recorded by lap timing. Final bleeding cessation was determined when no further bleeding occurred for 60 s. Mice that bled for 900 s were immediately cauterized and considered the maximal end point.

Platelet Spreading Assay. Cover glass was coated with 10 μg/mL vitronectin (Advanced BioMatrix) overnight at 4 °C and washed three times with PBS. Washed human or mouse platelets (4×10^6) were incubated on the matrix-coated glass for various times at 37 °C in the presence of dimethylsulfoxide (DMSO), 10 μM GPR56-AP, 10 μM GPR56-AP point mutant peptide, or 50 μM PAR4-AP. After PBS rinsing, adherent and spread platelets were fixed with 4% wt/vol paraformaldehyde, permeabilized with 0.05% wt/vol Triton X-100, blocked with 3% wt/vol BSA in PBS, incubated for 1 h with Phalloidin–Alexa-Fluor 488 diluted 1/1,000 vol/vol in PBS, and then washed three times with PBS. Images were acquired using a Leica confocal microscope equipped with 40×/1.3 or 100×/1.4 oil objectives. For adherent platelet counting, 15 image fields 40× magnified were quantified using ImageJ (NIH) cell counter plugin and plotted in terms of number of cells per unit area using GraphPad software (Prism).

Platelet Adhesion to Immobilized Collagen Flow Chamber Assays. Flow chambers μ-slide VI 0.1 mL (1 × 17 mm; Ibidi) were coated with 50 μg/mL equine collagen (Chronolog) for 18 h at 4 °C. Heparinized and 40 μM D-phenylalanyl-*N*-[(1S)-4-[(aminoiminomethyl)amino]-1-(2-chloroacetyl)butyl]-L-prolinamide (PPACK) (Cayman Chemical)-treated mouse or human whole blood was treated with 1 μM DiOC6 (ThermoFisher Scientific) for 15 min at 37 °C. The blood was perfused over the immobilized collagen at typical arterial (1,800 s^{-1}) or venous

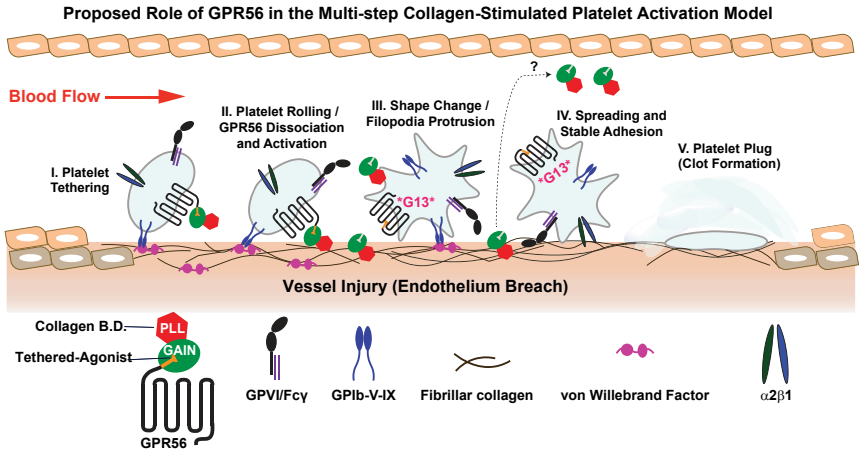

Fig. 8. Proposed model of platelet GPR56 activation in hemostasis. Upon damage to the vessel wall endothelium, the subendothelial connective tissue that contains collagen becomes exposed to circulation. The collagen rapidly recruits and helps to decelerate a few circulating platelets and induces their shape change and activation program. Tethering of platelets is mediated by interaction of collagen-bound vWF and the nonsignaling platelet glycoprotein, GP1b-V-IX. Platelets roll or translocate along the collagen through vWF/GP1b-V-IX interactions. During the rolling phase, we propose that platelet GPR56 interacts with collagen via its NTF PLL domain. Continued rolling of the platelet may provide sufficient shear force to dissociate the collagen-anchored GPR56 NTF from the platelet membrane-associated CTF. The NTF is jettisoned onto collagen, whereas the CTF is rapidly self-activated by tethered agonism to stimulate G13 signaling and induction of platelet shape changes and filopodia protrusion. The collagen-bound GPR56 NTF may become solubilized into the plasma for its clearance (dashed line). Shape change is a prerequisite to platelet spreading, firm adhesion, and the reinforcing signaling events mediated by other collagen receptors, including GPVI/FcRγ and integrin α2β1. Additional circulating platelets are recruited to the growing platelet plug, and secondary hemostasis ensues. GAIN, G protein-coupled receptor autoproteolysis-inducing domain.

shear (400 s^{-1}) rates as described (65, 90). Venous and arterial shear rates were controlled using an automated syringe pump (Harvard Apparatus), and fluorescently labeled platelet adhesion was monitored in real time using the 40× objective equipped on a Zeiss Axiovert 200M inverted fluorescent microscope. Platelet adhesion real-time videos were analyzed using Slidebook (3i).

Calcium Release Measurements. Washed human platelets at 3×10^8/mL were treated with 1 mM probenecid (ThermoFisher Scientific) for 30 min at 37 °C and loaded with 4.5 μM Fluo-4-AM (ThermoFisher Scientific) for 10 min at room temperature. Extracellular $CaCl_2$ was adjusted to 0.5 mM immediately prior to distributing 80-μL suspensions of platelets per well in 96-well plates. Basal Fluo4-AM fluorescence intensity was recorded for 30 s prior to the addition of agonists (20 μL each) at the indicated concentrations, prior to measurement of calcium responses (Hamamtsu FDSS7000EX).

Rho-GTP Production Assay. Human or mouse platelets at 5×10^8 in 500 μL of Tyrode's were stimulated with DMSO vehicle or GPR56 agonists in the presence of DMSO (vehicle control) or the GPR56 antagonist, DHM, for 90 s. Stimulation was quenched by addition of an equal volume of lysis buffer (100 mM Tris, pH 7.4, 150 mM NaCl, 2% wt/vol octylphenoxypolyethoxyethanol (IGEPAL), 1% wt/vol sodium deoxycholate, 0.05% wt/vol SDS, 2 mM Na_3VO_4, 2 mM phenylmethylsulfonyl fluoride, 2 mg/mL leupeptin, 2 mg/mL aprotinin). Samples were immediately vortexed and centrifuged at 21,000 × *g* for 1 min at 4 °C. Lysates were batch bound to 60 μg of Rhotekin-RBD beads (Cytoskeleton, Inc.) for 90 min at 4 °C. The beads were washed five times with lysis buffer and resuspended in 30 μL of Laemmli sample buffer. Bead-isolated RhoA-GTP and total lysate inputs were resolved by SDS/PAGE and immunoblotted with the RhoA antibody. The relative levels of RhoA-GTP were normalized to the total RhoA signal.

Adenylate Cyclase Assay. Human platelets were washed in Tyrode's buffer, adjusted to 8×10^6/mL, and incubated with 50 μM 3-isobutyl-1-methylxanthine (Enzo Life Sciences) for 30 min at 22 °C prior to treatment with DMSO (vehicle control), 56-AP, or ADP for 30 s at 22 °C. At 30 s, 10 μM forskolin (Sigma-Aldrich) and 10 nM PGI_2 (Sigma-Aldrich) were added, and the reactions were quenched at the indicated times with 0.1 M HCl (lysis buffer). Samples were vortexed and centrifuged at 21,000 × *g* for 5 min at 4 °C. The supernatants were collected for cAMP measurement using the direct cAMP ELISA kit (Enzo Life Sciences).

Data Availability. All study data are included in the article and *SI Appendix*.

ACKNOWLEDGMENTS. We thank Venkatesha Basrur and Alexey Nesvizhskii in the University of Michigan Proteomic Resource Facility within the Department of Pathology; and Alan V. Smrcka for advice and use of his confocal microscope. J.Y. acknowledges support from NIH Grants T32-HL007853 and F32HL14928001. A.V. acknowledges support from NIH Grant T32-GM007315. X.P. acknowledges support from National Institute of Neurological Disorders and Stroke Grants NS094164 and NS108446. M.H. acknowledges support from NIH Grants GM131835 and HL144660. G.G.T. acknowledges support from NIH Grants GM120110, GM088242, and NS103946.

1. B. Estevez, X. Du, New concepts and mechanisms of platelet activation signaling. *Physiology* **32**, 162–177 (2017).
2. S. P. Jackson, Arterial thrombosis–Insidious, unpredictable and deadly. *Nat. Med.* **17**, 1423–1436 (2011).
3. S. P. Watson, Platelet activation by extracellular matrix proteins in haemostasis and thrombosis. *Curr. Pharm. Des.* **15**, 1358–1372 (2009).
4. J. M. Gibbins, Platelet adhesion signalling and the regulation of thrombus formation. *J. Cell Sci.* **117**, 3415–3425 (2004).
5. B. Savage, E. Saldívar, Z. M. Ruggeri, Initiation of platelet adhesion by arrest onto fibrinogen or translocation on von Willebrand factor. *Cell* **84**, 289–297 (1996).
6. S. Watson, O. Berlanga, D. Best, J. Frampton, Update on collagen receptor interactions in platelets: Is the two-state model still valid? *Platelets* **11**, 252–258 (2000).
7. B. Nieswandt, S. P. Watson, Platelet-collagen interaction: Is GPVI the central receptor? *Blood* **102**, 449–461 (2003).
8. J. Rayes, S. P. Watson, B. Nieswandt, Functional significance of the platelet immune receptors GPVI and CLEC-2. *J. Clin. Invest.* **129**, 12–23 (2019).
9. M. J. Maxwell, S. M. Dopheide, S. J. Turner, S. P. Jackson, Shear induces a unique series of morphological changes in translocating platelets: Effects of morphology on translocation dynamics. *Arterioscler. Thromb. Vasc. Biol.* **26**, 663–669 (2006).
10. S. P. Jackson, The growing complexity of platelet aggregation. *Blood* **109**, 5087–5095 (2007).
11. S. P. Jackson, W. S. Nesbitt, S. Kulkarni, Signaling events underlying thrombus formation. *J. Thromb. Haemost.* **1**, 1602–1612 (2003).
12. S. Massberg *et al.*, A crucial role of glycoprotein VI for platelet recruitment to the injured arterial wall in vivo. *J. Exp. Med.* **197**, 41–49 (2003).
13. B. Nieswandt *et al.*, Glycoprotein VI but not alpha2beta1 integrin is essential for platelet interaction with collagen. *EMBO J.* **20**, 2120–2130 (2001).
14. Y. S. Bynagari-Settipalli *et al.*, Redundancy and interaction of thrombin- and collagen-mediated platelet activation in tail bleeding and carotid thrombosis in mice. *Arterioscler. Thromb. Vasc. Biol.* **34**, 2563–2569 (2014).
15. K. Kato *et al.*, The contribution of glycoprotein VI to stable platelet adhesion and thrombus formation illustrated by targeted gene deletion. *Blood* **102**, 1701–1707 (2003).
16. M. Bender *et al.*, Combined in vivo depletion of glycoprotein VI and C-type lectin-like receptor 2 severely compromises hemostasis and abrogates arterial thrombosis in mice. *Arterioscler. Thromb. Vasc. Biol.* **33**, 926–934 (2013).
17. M. G. Tomlinson *et al.*, Collagen promotes sustained glycoprotein VI signaling in platelets and cell lines. *J. Thromb. Haemost.* **5**, 2274–2283 (2007).
18. A. Moers *et al.*, G13 is an essential mediator of platelet activation in hemostasis and thrombosis. *Nat. Med.* **9**, 1418–1422 (2003).
19. B. Klages, U. Brandt, M. I. Simon, G. Schultz, S. Offermanns, Activation of G12/G13 results in shape change and Rho/Rho-kinase-mediated myosin light chain phosphorylation in mouse platelets. *J. Cell Biol.* **144**, 745–754 (1999).
20. T. Iguchi *et al.*, Orphan G protein-coupled receptor GPR56 regulates neural progenitor cell migration via a G alpha 12/13 and Rho pathway. *J. Biol. Chem.* **283**, 14469–14478 (2008).
21. R. Luo *et al.*, G protein-coupled receptor 56 and collagen III, a receptor-ligand pair, regulates cortical development and lamination. *Proc. Natl. Acad. Sci. U.S.A.* **108**, 12925–12930 (2011).

22. K. J. Paavola, J. R. Stephenson, S. L. Ritter, S. P. Alter, R. A. Hall, The N terminus of the adhesion G protein-coupled receptor GPR56 controls receptor signaling activity. *J. Biol. Chem.* **286**, 28914–28921 (2011).
23. H. M. Stoveken, A. G. Hajduczok, L. Xu, G. G. Tall, Adhesion G protein-coupled receptors are activated by exposure of a cryptic tethered agonist. *Proc. Natl. Acad. Sci. U.S.A.* **112**, 6194–6199 (2015).
24. D. Araç *et al*., A novel evolutionarily conserved domain of cell-adhesion GPCRs mediates autoproteolysis. *EMBO J.* **31**, 1364–1378 (2012).
25. I. Liebscher *et al*., A tethered agonist within the ectodomain activates the adhesion G protein-coupled receptors GPR126 and GPR133. *Cell Rep.* **9**, 2018–2026 (2014).
26. K. J. Paavola, H. Sidik, J. B. Zuchero, M. Eckart, W. S. Talbot, Type IV collagen is an activating ligand for the adhesion G protein–coupled receptor GPR126. *Sci. Signal.* **7**, ra76 (2014).
27. H. M. Stoveken, S. D. Larsen, A. V. Smrcka, G. G. Tall, Gedunin- and Khivorin-derivatives are small-molecule partial agonists for adhesion G protein-coupled receptors GPR56/ADGRG1 and GPR114/ADGRG5. *Mol. Pharmacol.* **93**, 477–488 (2018).
28. F. Bassilana, M. Nash, M. G. Ludwig, Adhesion G protein-coupled receptors: Opportunities for drug discovery. *Nat. Rev. Drug Discov.* **18**, 869–884 (2019).
29. R. Luo *et al*., Mechanism for adhesion G protein-coupled receptor GPR56-mediated RhoA activation induced by collagen III stimulation. *PLoS One* **9**, e100043 (2014).
30. G. S. Salzman *et al*., Structural basis for regulation of GPR56/ADGRG1 by its alternatively spliced extracellular domains. *Neuron* **91**, 1292–1304 (2016).
31. K. D. Little, M. E. Hemler, C. S. Stipp, Dynamic regulation of a GPCR-tetraspanin-G protein complex on intact cells: Central role of CD81 in facilitating GPR56-Galpha q/11 association. *Mol. Biol. Cell* **15**, 2375–2387 (2004).
32. J. Yeung, W. Li, M. Holinstat, Platelet signaling and disease: Targeted therapy for thrombosis and other related diseases. *Pharmacol. Rev.* **70**, 526–548 (2018).
33. G. S. Salzman *et al*., *Stachel*-independent modulation of GPR56/ADGRG1 signaling by synthetic ligands directed to its extracellular region. *Proc. Natl. Acad. Sci. U.S.A.* **114**, 10095–10100 (2017).
34. H. M. Stoveken *et al*., Dihydromunduletone is a small-molecule selective adhesion G protein-coupled receptor antagonist. *Mol. Pharmacol.* **90**, 214–224 (2016).
35. L. Brass, Understanding and evaluating platelet function. *Hematology (Am. Soc. Hematol. Educ. Program)* **2010**, 387–396 (2010).
36. S. J. Shattil, M. Cunningham, J. A. Hoxie, Detection of activated platelets in whole blood using activation-dependent monoclonal antibodies and flow cytometry. *Blood* **70**, 307–315 (1987).
37. S. J. Shattil, J. A. Hoxie, M. Cunningham, L. F. Brass, Changes in the platelet membrane glycoprotein IIb.IIIa complex during platelet activation. *J. Biol. Chem.* **260**, 11107–11114 (1985).
38. H. Gong *et al*., G protein subunit Galpha13 binds to integrin alphaIIbbeta3 and mediates integrin "outside-in" signaling. *Science* **327**, 340–343 (2010).
39. B. Nieswandt, V. Schulte, A. Zywietz, M. P. Gratacap, S. Offermanns, Costimulation of Gi- and G12/G13-mediated signaling pathways induces integrin alpha IIbbeta 3 activation in platelets. *J. Biol. Chem.* **277**, 39493–39498 (2002).
40. R. T. Dorsam, S. Kim, J. Jin, S. P. Kunapuli, Coordinated signaling through both G12/13 and G(i) pathways is sufficient to activate GPIIb/IIIa in human platelets. *J. Biol. Chem.* **277**, 47588–47595 (2002).
41. E. M. Golebiewska, A. W. Poole, Platelet secretion: From haemostasis to wound healing and beyond. *Blood Rev.* **29**, 153–162 (2015).
42. K. M. Meyers, C. L. Seachord, H. Holmsen, J. B. Smith, D. J. Prieur, A dominant role of thromboxane formation in secondary aggregation of platelets. *Nature* **282**, 331–333 (1979).
43. H. Holmsen, H. J. Day, C. A. Setkowsky, Secretory mechanisms. Behaviour of adenine nucleotides during the platelet release reaction induced by adenosine diphosphate and adrenaline. *Biochem. J.* **129**, 67–82 (1972).
44. S. Offermanns, Activation of platelet function through G protein-coupled receptors. *Circ. Res.* **99**, 1293–1304 (2006).
45. B. E. Tourdot *et al*., Genetic variant in human PAR (Protease-Activated Receptor) 4 enhances thrombus formation resulting in resistance to antiplatelet therapeutics. *Arterioscler. Thromb. Vasc. Biol.* **38**, 1632–1643 (2018).
46. Y. Liu, N. L. Jennings, A. M. Dart, X. J. Du, Standardizing a simpler, more sensitive and accurate tail bleeding assay in mice. *World J. Exp. Med.* **2**, 30–36 (2012).
47. M. S. Saito *et al*., New approaches in tail-bleeding assay in mice: Improving an important method for designing new anti-thrombotic agents. *Int. J. Exp. Pathol.* **97**, 285–292 (2016).
48. M. Fattorutto, Evaluation of platelet aggregation in flow and platelet aggregometry during pregnancy. *Br. J. Anaesth.* **90**, 252 (2003).
49. Z. Xia, M. M. Frojmovic, Aggregation efficiency of activated normal or fixed platelets in a simple shear field: Effect of shear and fibrinogen occupancy. *Biophys. J.* **66**, 2190–2201 (1994).
50. B. Linnemann, J. Schwonberg, H. Mani, S. Prochnow, E. Lindhoff-Last, Standardization of light transmittance aggregometry for monitoring antiplatelet therapy: An adjustment for platelet count is not necessary. *J. Thromb. Haemost.* **6**, 677–683 (2008).
51. Z. M. Ruggeri, S. P. Jackson, "Platelet thrombus formation in flowing blood" in *Platelets*, A. D. Michelson, Ed. (Academic Press, San Diego, CA, ed. 3, 2013), chap. 20, pp. 399–423.
52. Y. Yuan *et al*., The von Willebrand factor-glycoprotein Ib/V/IX interaction induces actin polymerization and cytoskeletal reorganization in rolling platelets and glycoprotein Ib/V/IX-transfected cells. *J. Biol. Chem.* **274**, 36241–36251 (1999).
53. S. L. Cranmer *et al*., Glycoprotein (GP) Ib-IX-transfected cells roll on a von Willebrand factor matrix under flow. Importance of the GPib/actin-binding protein (ABP-280) interaction in maintaining adhesion under high shear. *J. Biol. Chem.* **274**, 6097–6106 (1999).
54. G.-W. Chang *et al*., The adhesion G protein-coupled receptor GPR56/ADGRG1 is an inhibitory receptor on human NK cells. *Cell Rep.* **15**, 1757–1770 (2016).
55. Y. Tokoro, Y. Yamada, S. I. Takayanagi, T. Hagiwara, 57R2A, a newly established monoclonal antibody against mouse GPR56, marks long-term repopulating hematopoietic stem cells. *Exp. Hematol.* **59**, 51–59.e1 (2018).
56. Y. M. Peng *et al*., Specific expression of GPR56 by human cytotoxic lymphocytes. *J. Leukoc. Biol.* **90**, 735–740 (2011).
57. W. Y. Tseng *et al*., High levels of soluble GPR56/ADGRG1 are associated with positive rheumatoid factor and elevated tumor necrosis factor in patients with rheumatoid arthritis. *J. Microbiol. Immunol. Infect.* **51**, 485–491 (2018).
58. M. K. Delaney, J. Liu, Y. Zheng, M. C. Berndt, X. Du, The role of Rac1 in glycoprotein Ib-IX-mediated signal transduction and integrin activation. *Arterioscler. Thromb. Vasc. Biol.* **32**, 2761–2768 (2012).
59. X. Du, Signaling and regulation of the platelet glycoprotein Ib-IX-V complex. *Curr. Opin. Hematol.* **14**, 262–269 (2007).
60. I. Canobbio, C. Balduini, M. Torti, Signalling through the platelet glycoprotein Ib-V-IX complex. *Cell. Signal.* **16**, 1329–1344 (2004).
61. P. Lova, I. Canobbio, G. F. Guidetti, C. Balduini, M. Torti, Thrombin induces platelet activation in the absence of functional protease activated receptors 1 and 4 and glycoprotein Ib-IX-V. *Cell. Signal.* **22**, 1681–1687 (2010).
62. E. E. Gardiner *et al*., GPIbalpha-selective activation of platelets induces platelet signaling events comparable to GPVI activation events. *Platelets* **21**, 244–252 (2010).
63. P. Mangin *et al*., Signaling role for phospholipase C gamma 2 in platelet glycoprotein Ib alpha calcium flux and cytoskeletal reorganization. Involvement of a pathway distinct from FcR gamma chain and Fc gamma RIIA. *J. Biol. Chem.* **278**, 32880–32891 (2003).
64. S. P. Watson, J. M. Auger, O. J. T. McCarty, A. C. Pearce, GPVI and integrin αIIbβ3 signaling in platelets. *J. Thromb. Haemost.* **3**, 1752–1762 (2005).
65. A. J. Reininger *et al*., Mechanism of platelet adhesion to von Willebrand factor and microparticle formation under high shear stress. *Blood* **107**, 3537–3545 (2006).
66. S. M. Jung, M. Moroi, Signal-transducing mechanisms involved in activation of the platelet collagen receptor integrin alpha(2)beta(1). *J. Biol. Chem.* **275**, 8016–8026 (2000).
67. M. Moroi, I. Onitsuka, T. Imaizumi, S. M. Jung, Involvement of activated integrin alpha2beta1 in the firm adhesion of platelets onto a surface of immobilized collagen under flow conditions. *Thromb. Haemost.* **83**, 769–776 (2000).
68. J. M. Pasquet *et al*., LAT is required for tyrosine phosphorylation of phospholipase cgamma2 and platelet activation by the collagen receptor GPVI. *Mol. Cell. Biol.* **19**, 8326–8334 (1999).
69. N. A. Bezman *et al*., Requirements of SLP76 tyrosines in ITAM and integrin receptor signaling and in platelet function in vivo. *J. Exp. Med.* **205**, 1775–1788 (2008).
70. N. Y. Chiang *et al*., Heparin interacts with the adhesion GPCR GPR56, reduces receptor shedding, and promotes cell adhesion and motility. *J. Cell Sci.* **129**, 2156–2169 (2016).
71. S. Giera *et al*., Microglial transglutaminase-2 drives myelination and myelin repair via GPR56/ADGRG1 in oligodendrocyte precursor cells. *eLife* **7**, e33385 (2018).
72. O. E. Olaniru *et al*., The adhesion receptor GPR56 is activated by extracellular matrix collagen III to improve β-cell function. *Cell. Mol. Life Sci.* **75**, 4007–4019 (2018).
73. L. Badimon, J. J. Badimon, V. T. Turitto, S. Vallabhajosula, V. Fuster, Platelet thrombus formation on collagen type I. A model of deep vessel injury. Influence of blood rheology, von Willebrand factor, and blood coagulation. *Circulation* **78**, 1431–1442 (1988).
74. F. T. Bosman, I. Stamenkovic, Functional structure and composition of the extracellular matrix. *J. Pathol.* **200**, 423–428 (2003).
75. T. Kanaji, S. Russell, J. Ware, Amelioration of the macrothrombocytopenia associated with the murine Bernard-Soulier syndrome. *Blood* **100**, 2102–2107 (2002).
76. L. A. Bergmeier, T. Lehner, Innate and adaptive mucosal immunity in protection against HIV infection. *Adv. Dent. Res.* **19**, 21–28 (2006).
77. W. Bergmeier *et al*., The role of platelet adhesion receptor GPIbalpha far exceeds that of its main ligand, von Willebrand factor, in arterial thrombosis. *Proc. Natl. Acad. Sci. U.S.A.* **103**, 16900–16905 (2006).
78. P. Dunér *et al*., Adhesion G protein-coupled receptor G1 (ADGRG1/GPR56) and pancreatic β-Cell function. *J. Clin. Endocrinol. Metab.* **101**, 4637–4645 (2016).
79. K. Singer, R. Luo, S.-J. Jeong, X. Piao, GPR56 and the developing cerebral cortex: Cells, matrix, and neuronal migration. *Mol. Neurobiol.* **47**, 186–196 (2013).
80. J. P. White *et al*., G protein-coupled receptor 56 regulates mechanical overload-induced muscle hypertrophy. *Proc. Natl. Acad. Sci. U.S.A.* **111**, 15756–15761 (2014).
81. N.-Y. Chiang *et al*., Disease-associated GPR56 mutations cause bilateral frontoparietal polymicrogyria via multiple mechanisms. *J. Biol. Chem.* **286**, 14215–14225 (2011).
82. X. Piao *et al*., G protein-coupled receptor-dependent development of human frontal cortex. *Science* **303**, 2033–2036 (2004).
83. S. Giera *et al*., The adhesion G protein-coupled receptor GPR56 is a cell-autonomous regulator of oligodendrocyte development. *Nat. Commun.* **6**, 6121 (2015).
84. A. Reheman *et al*., Vitronectin stabilizes thrombi and vessel occlusion but plays a dual role in platelet aggregation. *J. Thromb. Haemost.* **3**, 875–883 (2005).
85. A. Reheman *et al*., Plasma fibronectin depletion enhances platelet aggregation and thrombus formation in mice lacking fibrinogen and von Willebrand factor. *Blood* **113**, 1809–1817 (2009).
86. Y. Wang *et al*., Plasma fibronectin supports hemostasis and regulates thrombosis. *J. Clin. Invest.* **124**, 4281–4293 (2014).
87. V. Proulle, R. A. Furie, G. Merrill-Skoloff, B. C. Furie, B. Furie, Platelets are required for enhanced activation of the endothelium and fibrinogen in a mouse thrombosis model of APS. *Blood* **124**, 611–622 (2014).
88. A. Sharda *et al*., Defective PDI release from platelets and endothelial cells impairs thrombus formation in Hermansky-Pudlak syndrome. *Blood* **125**, 1633–1642 (2015).
89. W. Li, T. M. McIntyre, R. L. Silverstein, Ferric chloride-induced murine carotid arterial injury: A model of redox pathology. *Redox Biol.* **1**, 50–55 (2013).
90. R. Polanowska-Grabowska, J. M. Gibbins, A. R. Gear, Platelet adhesion to collagen and collagen-related peptide under flow: Roles of the [alpha]2[beta]1 integrin, GPVI, and Src tyrosine kinases. *Arterioscler. Thromb. Vasc. Biol.* **23**, 1934–1940 (2003).